
MDDM: A MOLECULAR DYNAMICS DIFFUSION MODEL TO PREDICT PARTICLE SELF-ASSEMBLY

Kevin Ferguson Yu-hsuan Chen Levent Burak Kara

Department of Mechanical Engineering

Carnegie Mellon University

5000 Forbes Ave, Pittsburgh, PA 15213

{kferguso, yuhsuan2, lkara}@andrew.cmu.edu

ABSTRACT

The discovery and study of new material systems relies on molecular simulations that often come with significant computational expense. We propose MDDM, a Molecular Dynamics Diffusion Model, which is capable of predicting a valid output conformation for a given input pair potential function. After training MDDM on a large dataset of molecular dynamics self-assembly results, the proposed model can convert uniform noise into a meaningful output particle structure corresponding to an arbitrary input potential. The model’s architecture has domain-specific properties built-in, such as satisfying periodic boundaries and being invariant to translation. The model significantly outperforms the baseline point-cloud diffusion model for both unconditional and conditional generation tasks.

1 Introduction

Molecular Dynamics (MD) is a powerful computational tool that lets scientists and engineers study chemical, biological, or material systems at a micro- or nano-scale. In particular, we target a materials science application of molecular self-assembly in which the goal is to model the dynamics and structure of bulk systems containing many particles that interact with one another via a specified potential energy function. By simulating the motion and interaction of particles in a molecular system, material properties can be measured from the resulting equilibrated particle structures.

While MD undoubtedly provides engineers with the capacity to perform high-fidelity material simulations, it is not without its own limitations, namely computational expense. For one, very large systems (i.e. with many particles) are required to emulate the properties of a bulk material as accurately as possible. Crucially, the number of particle-to-particle interactions in a system scales quadratically with the number of particles. While each time step’s computations can be parallelized across multiple processors, the time-evolving nature of an MD simulation is inherently serial, leading to prohibitively lengthy simulation times.

In this work, we propose a denoising diffusion probabilistic model (for short, a diffusion model) that can act as a surrogate model for large-scale MD. A diffusion model starts with noise, and – through an iterative denoising process – generates a sample from the dataset distribution. Most often, diffusion models are image-generators, producing realistic images, often conditioned on a text prompt. In our proposed Molecular Dynamics Diffusion Model (MDDM), rather than creating an image from an input prompt, a set of particle locations is created from an input pair potential function.

We demonstrate both unconditional and conditional conformation generation for particle self-assembly. Our model properly accounts for the periodic boundary conditions present in MD. MDDM generates structures that match the target radial distribution functions qualitatively and quantitatively better than the baseline. By sampling from the MDDM model, the structure of materials systems can be obtained rapidly, with far fewer diffusion model denoising iterations (hundreds) compared to MD time steps (millions), letting an engineer study bulk material systems faster than ever before.

Our key contributions can be summarized as follows:

1. A large dataset of MD simulation results spanning a range of input system potentials and temperatures

2. MDDM, a Molecular Dynamics Diffusion Model that can generate a self-assembled structure from an input pairwise potential energy function
3. A periodic boundary graph network model suitable for denoising a particle configuration in a molecular dynamics context

2 Dataset and Task

2.1 Dataset

We have generated a large dataset of MD results for this problem using LAMMPS [1] because there is not an existing dataset for this task. The simulations consist of 1000 particles each within a $10 \times 10 \times 10$ box (units are dimensionless ‘LJ’ units). The system is annealed to the target temperature from a temperature 10× larger, and the pair potential is an *oscillating pair potential* given by $U_{\text{OPP}}(r) = r^{-15} + r^{-3} \cos(k(r - 1.25) - \phi)$, for parameters k and ϕ . Therefore, the inputs and outputs of the simulation are summarized as follows:

Inputs: Potential frequency k , Potential shift ϕ , Target system temperature T

Outputs: Final particle locations $\mathbf{X}_{(N \times 3)}$

We performed simulations across the parameter ranges: $1.0 \leq k \leq 15.0$; $0.0 \leq \phi \leq 6.0$; $0.01 \leq T \leq 0.05$, with 10 values across each input parameter, for a total of 1000 initial simulations. Visualizations of a few of these results are shown in Figure A1 in the Appendix.

2.2 Task and Evaluation Metric

The final goal is to, given the MD inputs from above, generate a set of particle locations that is indistinguishable from an MD trajectory output that had the same inputs. That is, the goal of MDDM will be to sample from the distribution of all possible output MD structures that correspond to a given input potential, temperature, and density. The necessary components are summarized in Fig. 1.

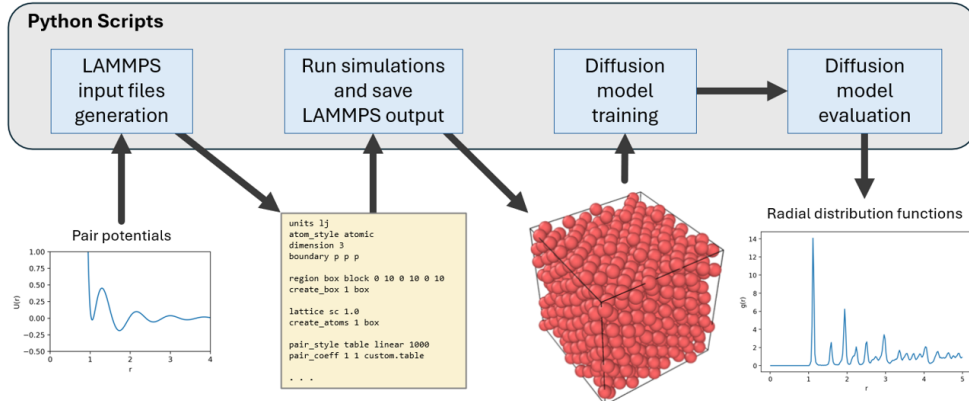


Figure 1: The dataset generation, model training, and model evaluation steps toward the MDDM task.

For an evaluation metric, we wish to compare the simulation structure output with those generated via our model. The radial distribution function (RDF) is a useful function that describes the normalized density of a particle system, with respect to a reference particle. RDFs are often visually compared to ensure no significant mismatch, as in [2]. For a more quantitative result, we use a loss function RDF-MSE, which computes the mean-squared-error between two RDF curves. We will also include RDF visualizations for comparison. This is especially important because visual inspection of particle structures themselves is infeasible, as is clear from Figure A1.

3 Related Work

Predicting the results of MD simulations is a highly sought-after task, often referred to as conformation generation [3]. Spellings et al. [4] characterize self-assembled molecular structures by classifying their phase, leveraging Gaussian

Mixture Models and various supervised learning techniques. While effective, they do not address the *generative* problem associated with creating a valid crystal structure. As for generative models, Arts et al. [5] use a diffusion model approach to predict the free energy coarse-grained MD structures, while Wu et al. [6] generate the steady-state conformation of molecules given their connectivity graphs. These approaches are similar to ours, but fail to solve a large-scale self-assembly generation task, as their simulations contain only a few dozen particles, rather than hundreds/thousands. Some authors attempt the inverse problem, trying to recover a suitable potential for a given output simulation [7, 8, 9]. However, these are iterative methods that require performing simulations in-the-loop. A generative surrogate would significantly accelerate such processes.

While the specific problem we pose has not been tackled using Generative AI, generative denoising diffusion models in the point-cloud domain have indeed been recently explored in a number of areas, such as high-energy physics simulation [10], anatomical reconstruction [11], and protein backbone generation [12]. Point-cloud diffusion models can also generate point clouds of common objects, having been trained on their respective shape datasets [13, 14]. Earlier, GANs were used for the same purpose [15]. These methods make use of point cloud encoders such as PointNet [16]. Other methods such as graph networks [17] or transformer-based approaches [18] can be used for this intermediate task as well.

4 Methods

In this section, we define the proposed MDDM model and outline procedures for training and sampling from the model. We also define a baseline to compare our method against.

Our approach is a denoising diffusion probabilistic model that operates in the 3-D point domain (rather than on 2-D images, as is typical of diffusion models). The input to our denoising process will be a set of particle coordinates sampled at random. These particle locations will be passed into a noise predictor model along with k , ϕ , and T (the inputs to the MD system – akin to the text prompt in an image diffusion model). The resulting prediction is a displacement of each particle, which we add to the initial positions to yield the denoised positions. This denoising procedure is repeated T iterations, and the final output should be a particle conformation that corresponds to the inputs.

4.1 Benchmark

Due to of the lack of generative models for self-assembly in the MD domain, we compare against a somewhat disparate baseline: Diffusion with Transolver. That is, we use Transolver [18] as a means of iteratively denoising a point cloud from noise to structure. The node-embedding capabilities of Transolver make it ideal for processing an input shape and predicting a suitable noise vector at each node. We apply the same diffusion strategy for the baseline as we do for our proposed model, which was inspired in part by Diffusion Point Cloud [13].

4.2 Model Architecture

The diffusion model architecture is defined in analogy with image diffusion methods, as shown in Fig. 2.

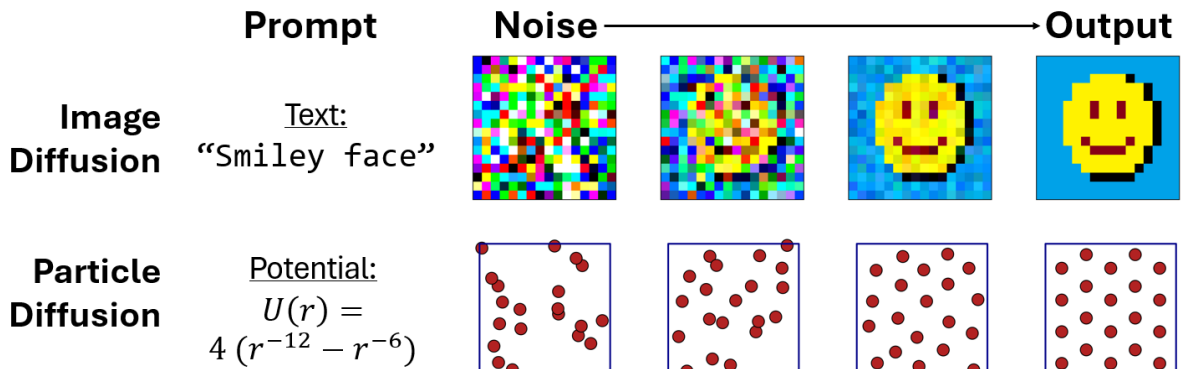


Figure 2: Text-conditioned image diffusion models, compared with the proposed potential-conditioned particle diffusion model for MD conformation generation

The denoising step has been designed specifically to operate in the presence of periodic boundary conditions. The full denoising model architecture is shown in Fig. 3 below.

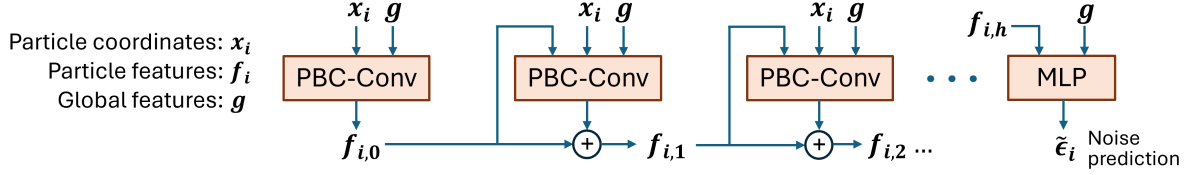


Figure 3: Denoising graph neural network architecture

Each PBC-Conv layer involves first creating a k -nearest neighbors graph in the periodic domain. We implement a set of terse, yet still further optimizable, functions in PyTorch [19] to generate this. Once generated for a set of particles, the same graph can be re-used for subsequent PBC-Conv layers, until the denoising step has been applied, modifying particle positions. Then Eqn. 1 is a learnable convolution function defined as follows:

$$\mathbf{f}'_i = \max_{j \in \mathcal{N}(i)} h_{\Theta}([\mathbf{x}_j - \mathbf{x}_i]_{\odot} \parallel \mathbf{f}_i \parallel \mathbf{f}_j - \mathbf{f}_i \parallel \mathbf{g}), \quad (1)$$

where \mathbf{f}'_i is the output convolved set of features of particle i , $\mathcal{N}(i)$ are the periodic k -nearest neighbors of particle i , $[\mathbf{x}_j - \mathbf{x}_i]_{\odot}$ refers to the vector from neighbor \mathbf{x}_j to source \mathbf{x}_i (wrapped across periodic boundaries as needed), \mathbf{f}_i is the input pre-convolution set of features at particle i , and \mathbf{g} is the global feature vector; \mathbf{g} contains information about the MD system, such as potential parameters and temperature, as well as diffusion process parameters, like diffusion fraction t/T . This function is based on the EdgeConv operation from Wang et al. [17], but accounts for periodic boundaries and does not explicitly pass absolute coordinates into the model, making our model translation-invariant (also a property of MD simulations).

Our network consists of 8 PBC-Conv layers with hidden local/global feature counts of 32 at each layer, using a periodic k -nearest neighbors graph with $k = 32$. Each PBC-Conv layer contains an MLP with 2 hidden layers of 32 neurons each. The output MLP has 2 layers, each with 128 neurons. The sole global input was t/T , current diffusion time step divided by the total number of diffusion steps, with $T = 500$ for our experiments.

4.3 Training and Sampling

For a standard image-based DDPM, the forward diffusion step is given by:

$$\mathbf{x}_t = \sqrt{\alpha_t} \mathbf{x}_0 + \sqrt{1 - \alpha_t} \boldsymbol{\epsilon}, \quad \text{for } \boldsymbol{\epsilon} \sim \mathcal{N}(\mathbf{0}, \mathbf{I}), \quad (2)$$

in which \mathbf{x}_0 is the data, \mathbf{x}_t is the data corrupted by t steps of diffusion, and α_t is a constant indicating the magnitude of diffusion from step 0 to step t . However, use of this equation is predicated on the notion that at the final diffusion step, pixel values are normally distributed. For our systems, due to the presence of PBCs, particle locations will not obey a normal distribution after diffusion. Rather, they will take on a (very nearly) uniform distribution, since wrapping a normal distribution makes it become approximately uniform. A proof of this statement can be found in the Appendix. Because the final noise is not normally distributed, the standard DDPM variational inference algorithm must be slightly reformulated. To do so, we redefine the forward diffusion process as follows:

$$\mathbf{x}_t = \mathbf{x}_0 + \sqrt{\alpha_t} \boldsymbol{\epsilon}, \quad \text{for } \boldsymbol{\epsilon} \sim \mathcal{N}(\mathbf{0}, \mathbf{I}) \quad (3)$$

Now, we can continue to use properties of Gaussians, and maximization of the Evidence Lower Bound (ELBO) during training can be re-derived for this revised formulation. Note that the result in Eqn. 3 is also wrapped within the periodic box domain. This gives rise to the training and sampling pseudocode below in Algorithms 1 and 2. A probabilistic derivation is provided in the Appendix.

Algorithm 1 Training

```

1: repeat
2:    $\mathbf{x}_0 \sim q(\mathbf{x}_0)$ 
3:    $t \sim \text{Uniform}(\{1, \dots, T\})$ 
4:    $\epsilon \sim \mathcal{N}(\mathbf{0}, \mathbf{I})$ 
5:    $\mathbf{x}_t \leftarrow \text{wrap}(\mathbf{x}_0 + \sqrt{\alpha_t} \epsilon)$ 
6:   Take optimizer step on  $L_2$  loss,  $\nabla_{\theta} \|\epsilon - \epsilon_{\theta}(\mathbf{x}_t, t)\|_2$ 
7: until converged

```

Algorithm 2 Sampling

```

1:  $\mathbf{x}_T \sim \mathcal{U}(0, L)$ 
2: for  $t = T, \dots, 1$  do
3:    $\mathbf{z} \sim \mathcal{N}(\mathbf{0}, \mathbf{I})$  if  $t > 1$ , else  $\mathbf{z} = \mathbf{0}$ 
4:    $\mu_t \leftarrow \left( \frac{\alpha_{t-1}}{\alpha_t} - 1 \right) \cdot (\sqrt{\alpha_t} \epsilon_{\theta}(\mathbf{x}_t, t)) + \mathbf{x}_t$ 
5:    $\sigma_t^2 \leftarrow \frac{\alpha_{t-1}}{2\alpha_t} (\alpha_t - \alpha_{t-1})$ 
6:    $\mathbf{x}_{t-1} \leftarrow \text{wrap}(\mu_t + \sigma_t \mathbf{z})$ 
7: return  $\mathbf{x}_0$ 

```

For our experiments, we use $T = 500$ diffusion steps with α on a cosine-schedule $\alpha_t = \cos^2\left(\frac{\pi}{2} \cdot \frac{x/(T+1)+s}{1+s}\right)$, with $s = 0.008$. We train for 800 epochs using an Adam optimizer with learning rate 0.005, which decreases by a factor of 0.95 every 100 epochs.

5 Experiments

We run experiments on two versions of the MD task: unconditional generation and conditional generation. For unconditional generation, we train each model to generate a single randomly-selected MD conformation from our dataset – no condition prompt is fed into the model. The dataset is augmented with rotated/flipped versions of this conformation to avoid memorization of coordinate locations. For conditional generation, we train models to generate valid output conformations given the k , ϕ , and T as additional input conditions, for the range of input parameters described in Sec. 2. We now present results for both models on unconditional and conditional tasks, with RDF-MSE results shown in Tab. 1.

Table 1: Performance, as measured by RDF-MSE, of our method compared to the baseline method.

Model	RDF-MSE Unconditional	RDF-MSE Conditional (Train)	RDF-MSE Conditional (Test)
Diff. w/ Transolver <i>MDDM (Ours)</i>	0.482 0.023	0.523 0.098	0.527 0.126

To evaluate our diffusion model, we pass a set of MD inputs into the model and compare the resulting structures using the radial distribution function (RDF). For the unconditional generation task, we see a close match between the generated outputs and the ground truth – this, and the low MSE value indicate that the denoising procedure can indeed perform conformation generation. The baseline, however, struggles to yield performance as strong as our model, likely due to it prioritizing recreation of global shape information rather than local structure.

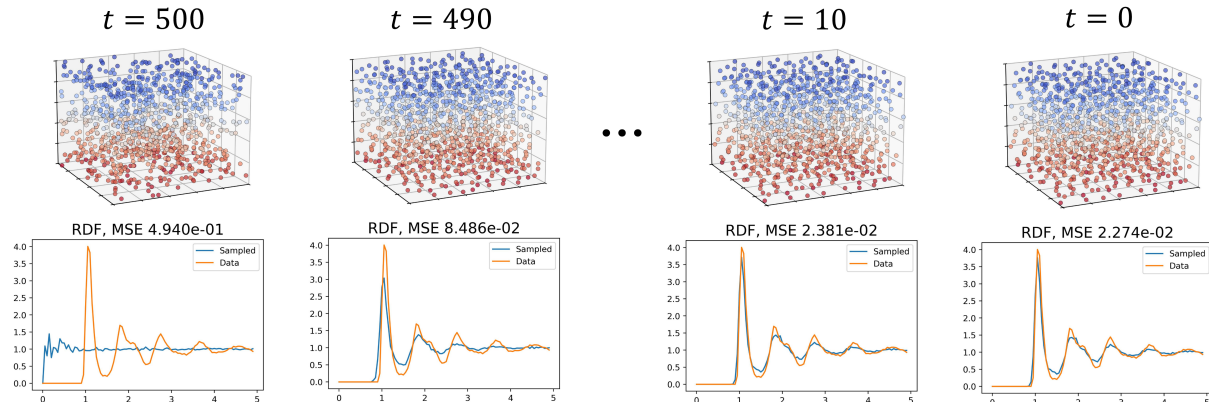


Figure 4: A demonstration of the sampling process for the unconditional generation task. The structure is mostly achieved in 10 diffusion steps, but RDF-MSE continues to decrease during subsequent steps

As for conditional generation, passing in potential as the input and using all 1000 MD results as training data (an additional 25 simulations for new parameters randomly sampled from the same range were used for testing), the results are promising, but leave room for improvement. Diffusion with Transolver still struggles for this task, but MDDM matches the first RDF peak well. Subsequent peaks, however, exhibit some mismatch, so there is still nuance to the conditional task that our model struggles to capture. To address this, starting with a smaller dataset, a larger model, or modified architecture (e.g. passing in the condition using cross-attention rather than concatenation), are a few strategies worth trying.

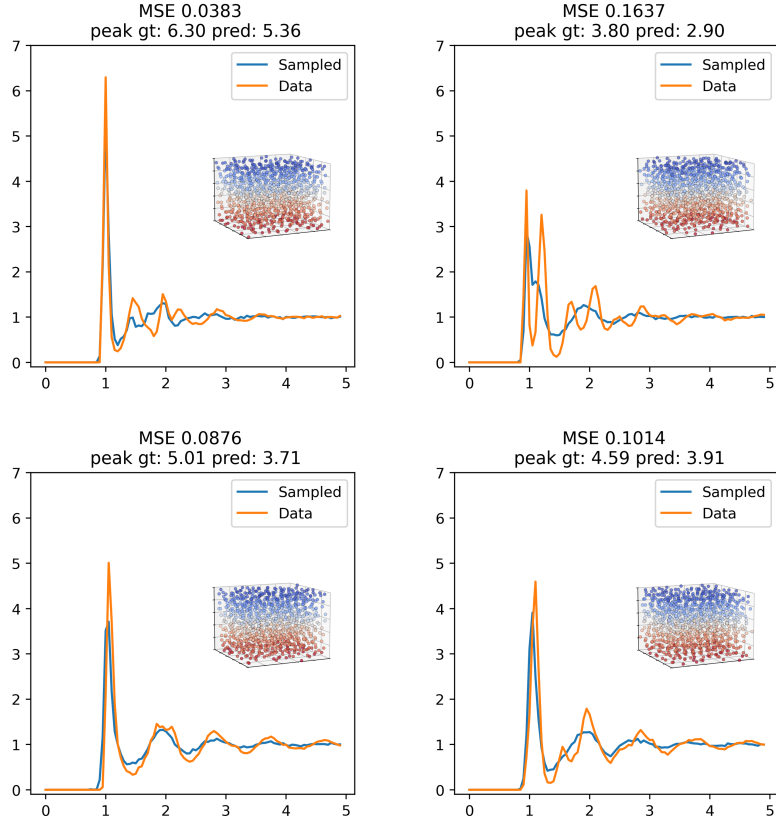


Figure 5: Four randomly selected results in the conditional generation task. Note the strong prediction of the first peak, followed by less accurate RDF match at larger length scales.

Using a single NVIDIA RTX A6000 GPU with 128GB DDR4 RAM, performance metrics were evaluated for two models: Transolver and PBCCConv. Transolver, with 128,867 parameters, achieved a training time of 24.03 seconds per 1,000 iterations and a sampling time of 2.53 seconds for 500 steps per data. In comparison, PBCCConv, with 101,891 parameters, recorded a slightly faster training time of 23.15 seconds per 1,000 iterations but a longer sampling time of 4.17 seconds for 500 steps per data. The increased sampling time for our method is potentially attributed to the repeated graph generation, which requires calculating each particle’s relative distance to its neighbors at every step. This added computational complexity likely contributes to the observed difference in sampling efficiency.

6 Conclusion

We recontextualize diffusion models in a new domain: conformation generation for molecular dynamics material self-assembly. The proposed MDDM model uses a custom periodic graph neural network to iteratively denoise uniformly distributed particles into meaningful structures. For training data, we generated a dataset of 1000 MD results for different input potentials and temperatures. MDDM significantly outperforms point-cloud-based diffusion models for MD particle conformation generation. Unconditional generation has strong results, but there is still room for improvement in the conditional generation task.

For future work, we hope to improve conditional generation; some possible avenues toward achieving this may include increasing the capacity of the model or redesigning the model architecture. Exploration of MD systems with non-isotropic and/or many-body potential functions would be another interesting extension of this work.

Acknowledgments

We thank the following individuals for their thoughtful discussion: Thomas O’Connor, Michael Bockstaller, Ayesha Abdullah, Andrew Gillman, Eric Harper, Jeffrey Ethier, Larry Drummy, Jacob Rast, and Matt Gormley.

References

- [1] A. P. Thompson, H. M. Aktulga, R. Berger, D. S. Bolintineanu, W. M. Brown, P. S. Crozier, P. J. in ’t Veld, A. Kohlmeyer, S. G. Moore, T. D. Nguyen, R. Shan, M. J. Stevens, J. Tranchida, C. Trott, and S. J. Plimpton. LAMMPS - a flexible simulation tool for particle-based materials modeling at the atomic, meso, and continuum scales. *Comp. Phys. Comm.*, 271:108171, 2022.
- [2] Zijie Li, Kazem Meidani, Prakarsh Yadav, and Amir Barati Farimani. Graph neural networks accelerated molecular dynamics. *The Journal of Chemical Physics*, 156(14):144103, 04 2022.
- [3] Paul C. D. Hawkins. Conformation generation: The state of the art. *Journal of Chemical Information and Modeling*, 57(8):1747–1756, 2017. PMID: 28682617.
- [4] Matthew Spellings and Sharon C. Glotzer. Machine learning for crystal identification and discovery. *AIChE Journal*, 64(6):2198–2206, June 2018.
- [5] Marloes Arts, Victor Garcia Satorras, Chin-Wei Huang, Daniel Zügner, Marco Federici, Cecilia Clementi, Frank Noé, Robert Pinsler, and Rianne van den Berg. Two for one: Diffusion models and force fields for coarse-grained molecular dynamics. *Journal of Chemical Theory and Computation*, 19(18):6151–6159, 2023. PMID: 37688551.
- [6] Fang Wu and Stan Z. Li. Diffmd: A geometric diffusion model for molecular dynamics simulations. *Proceedings of the AAAI Conference on Artificial Intelligence*, 37(4):5321–5329, Jun. 2023.
- [7] E. Edlund, O. Lindgren, and M. Nilsson Jacobi. Designing isotropic interactions for self-assembly of complex lattices. *Phys. Rev. Lett.*, 107:085503, Aug 2011.
- [8] E. Edlund, O. Lindgren, and M. Nilsson Jacobi. Novel self-assembled morphologies from isotropic interactions. *Phys. Rev. Lett.*, 107:085501, Aug 2011.
- [9] Carl S. Adorf, James Antonaglia, Julia Dshemuchadse, and Sharon C. Glotzer. Inverse design of simple pair potentials for the self-assembly of complex structures. *The Journal of Chemical Physics*, 149(20):204102, 11 2018.
- [10] Vinicius Mikuni, Benjamin Nachman, and Mariel Pettee. Fast point cloud generation with diffusion models in high energy physics. *Physical Review D*, 108(3):036025, 2023.
- [11] Paul Friedrich, Julia Wolleb, Florentin Bieder, Florian M. Thieringer, and Philippe C. Cattin. *Point Cloud Diffusion Models for Automatic Implant Generation*, page 112–122. Springer Nature Switzerland, 2023.
- [12] Jason Yim, Brian L. Trippe, Valentin De Bortoli, Emile Mathieu, Arnaud Doucet, Regina Barzilay, and Tommi Jaakkola. Se(3) diffusion model with application to protein backbone generation, 2023.
- [13] Shitong Luo and Wei Hu. Diffusion probabilistic models for 3d point cloud generation. In *Proceedings of the IEEE/CVF Conference on Computer Vision and Pattern Recognition (CVPR)*, pages 2837–2845, June 2021.
- [14] Xiaohui Zeng, Arash Vahdat, Francis Williams, Zan Gojcic, Or Litany, Sanja Fidler, and Karsten Kreis. Lion: Latent point diffusion models for 3d shape generation, 2022.
- [15] Chun-Liang Li, Manzil Zaheer, Yang Zhang, Barnabas Poczos, and Ruslan Salakhutdinov. Point cloud gan, 2018.
- [16] Charles R. Qi, Hao Su, Kaichun Mo, and Leonidas J. Guibas. Pointnet: Deep learning on point sets for 3d classification and segmentation, 2017.
- [17] Yue Wang, Yongbin Sun, Ziwei Liu, Sanjay E. Sarma, Michael M. Bronstein, and Justin M. Solomon. Dynamic graph cnn for learning on point clouds, 2019.
- [18] Haixu Wu, Huakun Luo, Haowen Wang, Jianmin Wang, and Mingsheng Long. Transolver: A fast transformer solver for pdes on general geometries, 2024.
- [19] Adam Paszke, Sam Gross, Soumith Chintala, Gregory Chanan, Edward Yang, Zachary DeVito, Zeming Lin, Alban Desmaison, Luca Antiga, and Adam Lerer. Automatic differentiation in pytorch, 2017.

[20] James Marengo, David Farnsworth, and Lucas Stefanic. A geometric derivation of the irwin-hall distribution. *International Journal of Mathematics and Mathematical Sciences*, 2017:1–6, 09 2017.

[21] Calvin Luo. Understanding diffusion models: A unified perspective. *arXiv preprint arXiv:2208.11970*, 2022.

Appendix A Figures

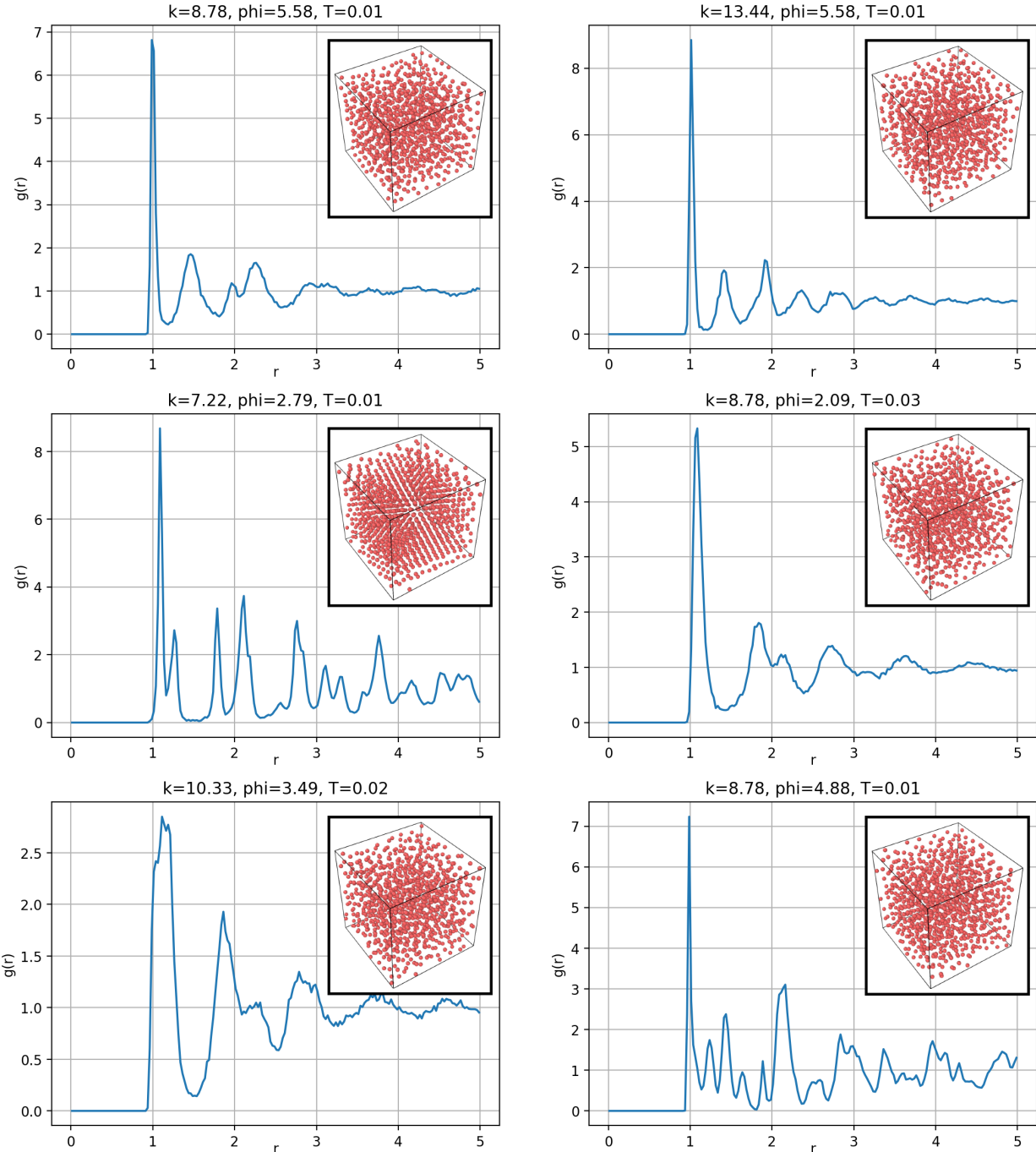


Figure A1: A sample gallery of radial distribution function (RDF) results and particle visualizations from the generated dataset. k and ϕ are parameters of the oscillating pair potential, while T is dimensionless temperature

Appendix B Shape generation task

To sanity-check our model and the baseline, we start by investigating two shape-generation tasks, which is a more natural task for Diffusion with Transolver, and typical of point-cloud generative models. We train each model to generate a unit sphere and simple torus from normally-distributed points by training them on points sampled uniformly on the surfaces of these shapes. The results are shown in Tab. A1. (Note that due to the translation-invariance of MDDM, we have re-centered the points after each diffusion step during sampling.) Sinkhorn loss, a metric for point-cloud matching, is reported.

Table A1: Sinkhorn loss for the sphere and torus generated by our model and the baseline

Model	Sinkhorn Loss Sphere	Sinkhorn Loss Torus
Diff. w/ Transolver	0.0746	0.0155
<i>MDDM (Ours)</i>	0.0796	0.0165

Figure A2 contains renders of the point clouds generated by each method, which were qualitatively successful. Table A1 reveals that our model performs nearly as well as the baseline for shape generation tasks. This indicates that both our model and the baseline are working as intended and can be trained on the MD task.

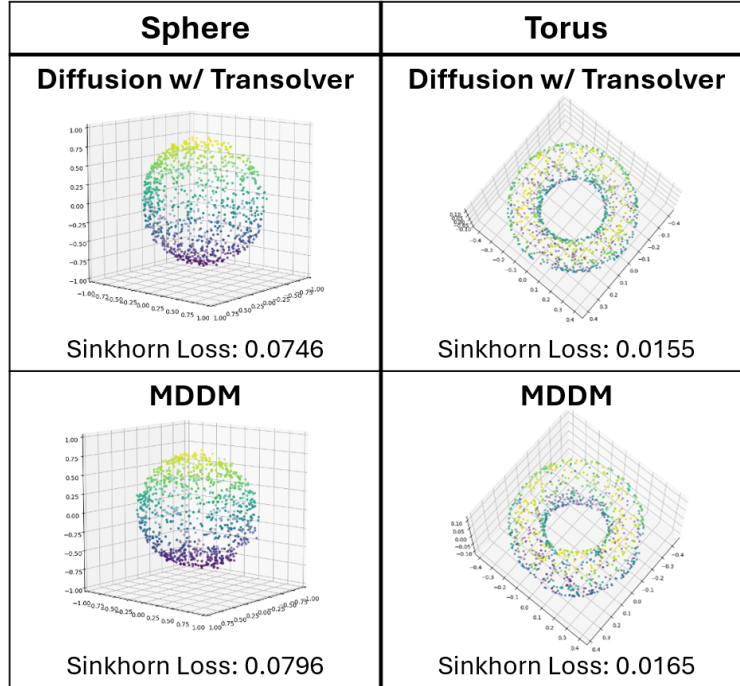


Figure A2: Sphere- and torus-matching results for our method and the baseline.

Appendix C Mathematical claims

Appendix C.1 Uniformity of a wrapped Gaussian

Claim 1. *A normal distribution with standard deviation L that has been wrapped by a periodic boundary function onto the interval $[0, L)$ approximates a uniform distribution on $[0, L)$.*

Proof. (Note: This proof does not quantify the error in the approximate result. However, our experiments have shown that the probability density function of a wrapped standard normal distribution is virtually indistinguishable from that of a uniform distribution at all points; the following proof explains why.)

We start by showing that the theorem holds for the standard normal distribution with mean 0 and standard deviation 1, and without loss of generality we assert that the result extends to other means and standard deviations.

Let X be a random variable with a standard normal distribution. According to the Central Limit Theorem, this can be closely approximated by an Irwin-Hall distribution with $N = 12$ (that is, the distribution describing the sum of 12 independent uniform random variables on $[0, 1]$, subtracting 6 here to re-center at zero), which has mean 0 and standard deviation 1 when expressed using the PDF below, adapted from Marengo et al. [20].

$$X \sim N(0, 1), \quad \frac{1}{\sqrt{2\pi}} e^{-\frac{x^2}{2}} \approx f_X(x) = \frac{1}{2(12-1)!} \sum_{r=0}^{12} (-1)^r \binom{12}{r} \operatorname{sgn}(x+6-r)(x+6-r)^{12-1}$$

Suppose $Y = g_L(X)$ is a periodic boundary function of X , where $g_L(a)$ is defined such that $g_L(a) = a + k_a L$, for the unique integer k_a such that $0 \leq g_L(a) < L$. We aim to derive the PDF of Y . For a general non-monotonic transformation, the PDF of Y is given by the change of variables:

$$f_Y(y) = \sum_{x: g_L(x)=y} \frac{f_X(x)}{|g_L'(x)|}.$$

Note that this sum accounts for all possible preimages $\forall k \in \mathbb{Z} : x = y + kL$, but $f_Y(y)$ is only nonzero on the interval $[0, 1)$, and only k values from -6 to 5 result in nonzero probability density. Also, $|g_L'(x)|$ evaluates to 1 everywhere. Thus, the sum is:

$$f_Y(y) = \begin{cases} \sum_{k=-6}^5 \frac{1}{2(12-1)!} \sum_{r=0}^{12} (-1)^r \binom{12}{r} \operatorname{sgn}(y+k+6-r)(y+k+6-r)^{12-1} & \text{if } 0 \leq y < 1, \\ 0 & \text{otherwise} \end{cases}$$

For y values on the interval $[0, 1)$, this expands to:

$$\begin{aligned} f_Y(y) \Big|_{0 \leq y < 1} &= \left(-462(y-6)^{11} + (y-1)^{11} + 11(y+1)^{11} - 55(y+2)^{11} + 165(y+3)^{11} \right. \\ &\quad + 330(y-5)^{11} - 55(y-10)^{11} - 11(y-2)^{11} + 11(y-11)^{11} + 55(y-3)^{11} \\ &\quad - 165(y+8)^{11} + 55(y+9)^{11} - 11(y+10)^{11} + (y+11)^{11} + 462(y-7)^{11} \\ &\quad - 330(y-8)^{11} - 165(y-4)^{11} + 165(y-9)^{11} - 330(y+4)^{11} + 462(y+5)^{11} \\ &\quad \left. - 462(y+6)^{11} + 330(y+7)^{11} - (y-12)^{11} - y^{11} \right) / (2(12-1)!) \\ &= 1 \end{aligned}$$

Through symbolic manipulation, the above expression evaluates to exactly 1. Therefore, the PDF is simply:

$$f_Y(y) = \begin{cases} 1 & \text{if } 0 \leq y < 1, \\ 0 & \text{otherwise} \end{cases}$$

This is recognized as a uniform distribution on $[0, 1)$. Therefore, because the wrapped Irwin-Hall distribution is exactly uniform, we conclude the distribution $\mathcal{N}(0, 1)$ wrapped onto the interval $[0, 1)$ closely approximates the uniform distribution $\mathcal{U}[0, 1)$.

Without loss of generality, this relationship holds for any mean μ and any standard deviation L by rescaling the distributions and shifting the periodic region. Thus, the distribution $\mathcal{N}(\mu, L)$ wrapped onto the interval $[0, L)$ approximates the uniform distribution $\mathcal{U}[0, L)$. ■

Appendix C.2 Variational Inference for a Reinterpretation of Diffusion

Claim 2. For a forward diffusion process defined by $\mathbf{x}_t = \mathbf{x}_0 + \sqrt{\alpha_t} \boldsymbol{\epsilon}$; $\boldsymbol{\epsilon} \sim \mathcal{N}(\mathbf{0}, \mathbf{I})$, the posterior mean for variational inference is $\mu_t = \frac{x_t - x_0}{\alpha_t} \alpha_{t-1} + x_0$ and the posterior variance is $\sigma_t^2 = \frac{\alpha_{t-1}(\alpha_t - \alpha_{t-1})}{2\alpha_t}$.

Proof. To start, we know the ELBO of the diffusion term [21] is

$$\begin{aligned} \mathbf{E}_{q(x_1:x_T|x_0)} \log \frac{p(x_0 : x_T)}{q(x_1 : x_T|x_0)} &= \mathbf{E}_{q(x_1|x_0)} \log P_\theta(x_0|x_1) - D_{KL}(q(x_1|x_0) || p(x_T)) \\ &\quad - \sum_{t=2}^T \mathbf{E}_{q(x_1|x_0)} (D_{KL}(q(x_{t-1}|x_t, x_0) || p_\theta(x_{t-1}|x_t))) \end{aligned} \quad (4)$$

For variational inference, we are interested in deriving a mathematical expression for the third term of this equation, the *denoising matching term*. In particular, we assume that q follows a Gaussian distribution, and we want to minimize the KL divergence. Therefore, the goal is to find the mean and variance of this distribution that would result in the closest possible match between distributions p and q . To do this, we first rewrite x_t and x_{t-1} in terms of our denoising process from 3 as follows:

$$\begin{aligned} x_t &= x_0 + \sqrt{\alpha_t} \boldsymbol{\epsilon} \\ x_{t-1} &= x_0 + \sqrt{\alpha_{t-1}} \boldsymbol{\epsilon} \\ x_t &= x_{t-1} + (\sqrt{\alpha_t} - \sqrt{\alpha_{t-1}}) \boldsymbol{\epsilon}, \end{aligned} \quad (5)$$

where $\boldsymbol{\epsilon} \sim \mathcal{N}(\mathbf{0}, \mathbf{I})$. Next, we look to Bayes' Rule to obtain a relationship between the conditional probabilities:

$$q(x_{t-1}|x_t, x_0) = \frac{q(x_t|x_{t-1}, x_0) q(x_{t-1}|x_0)}{q(x_t|x_0)} \quad (6)$$

Using the above equations, we can determine proportionality relationships in the denoising matching term:

$$\begin{aligned} &\frac{\mathcal{N}(x_t; x_{t-1}, (\alpha_t - \alpha_{t-1})\mathbf{I}) \cdot \mathcal{N}(x_{t-1}; x_0, \alpha_{t-1}\mathbf{I})}{\mathcal{N}(x_t; x_0, \alpha_t\mathbf{I})} \dots \\ &\propto \exp \left(- \left[\frac{(x_t - x_{t-1})^2}{\alpha_t - \alpha_{t-1}} + \frac{(x_{t-1} - x_0)^2}{\alpha_{t-1}} - \frac{(x_t - x_0)^2}{\alpha_t} \right] \right) \\ &\propto \exp \left(\frac{-1}{2} \left[\frac{2\alpha_t^2}{\alpha_t \alpha_{t-1} (\alpha_t - \alpha_{t-1})} \right] \left[x_{t-1}^2 - 2x_{t-1} \left(\frac{x_t - x_0}{\alpha_t} \alpha_{t-1} + x_0 \right) + \left(\frac{x_t - x_0}{\alpha_t} \alpha_{t-1} + x_0 \right)^2 \right] \right) \\ &\propto \mathcal{N} \left(x_{t-1}; \mu = \frac{x_t - x_0}{\alpha_t} \alpha_{t-1} + x_0, \sigma^2 = \frac{\alpha_{t-1}(\alpha_t - \alpha_{t-1})}{2\alpha_t} \right) \end{aligned} \quad (7)$$

Equation 7 therefore gives a formulation for mean and variance under our modified noising strategy. Note that to maintain training robustness, we regulate the training objective to always be distributed as $\mathcal{N}(\mathbf{0}, \mathbf{I})$. Therefore, during sampling, the mean becomes:

$$\mu = \frac{x_t - \hat{x}_0}{\alpha_t} \alpha_{t-1} + \hat{x}_0 = \left(\frac{\alpha_{t-1}}{\alpha_t} - 1 \right) \cdot (\sqrt{\alpha_t} \boldsymbol{\epsilon}_\theta(\mathbf{x}_t, t)) + \mathbf{x}_t \quad (8)$$

The mean and standard deviation in Eqns. 7 and 8 are then used during sampling (Algorithm 2). ■